Sheikh *et al. J Wireless Com Network* (2021) 2021:81
https://doi.org/10.1186/s13638-021-01965-9

EURASIP Journal on Wireless Communications and Networking

RESEARCH Open Access

A study about signal variation with minor receiver displacement in a meeting room at 60 GHz: measurements and simulations

Muhammad Usman Sheikh*, Kalle Ruttik, Riku Jäntti and Jyri Hämäläinen

*Correspondence: muhammad.sheikh@aalto.fi
Department of Communications and Networking, Aalto University, 02150 Espoo, Finland

Abstract

The aim of this work is to study the impact of small receiver displacement on a signal propagation in a typical conference room environment at a millimeter wave frequency of 60 GHz. While channel measurements provide insights on the propagation phenomena, their use for the wireless system performance evaluation is challenging. Whereas, carefully executed three-dimensional ray tracing (RT) simulations represent a more flexible option. Nevertheless, a careful validation of simulation methodology is needed. The first target of this article is to highlight the benefits of an in-house built three-dimensional RT tool at 60 GHz and shows the effectiveness of simulations in predicting different characteristics of the channel. To validate the simulation results against the measurements, two different transmitter (Tx) positions and antenna types along with ten receiver (Rx) positions are considered in a typical conference room. In first system configuration, an omnidirectional antenna is placed in the middle of the table, while in the second system configuration a directed horn antenna is located in the corner of the meeting room. After validating the simulation results with the measurement data, in the second part of this work, the impact of a small change, i.e., 20 cm in the receiver position, is studied. To characterize the impact, we apply as performance indicators the received power level, root mean square delay spread (RMS-DS) and RMS angular spread (RMS-AS) in azimuth plane. The channel characteristics are considered with respect to the direct orientation (DO), i.e., the Rx antenna is directed toward the strongest incoming path. Different antenna configurations at the Tx and Rx side are applied to highlight the role of antenna properties on the considered channel characteristics. Especially, in the second system configuration the impact of different antenna half power beamwidth on different considered channel characteristics is highlighted through acquired simulation results. The validation of results shows the RMS error of only 2–3 dB between the measured and simulated received power levels for different Tx configurations in the direction of DO. Results indicate that only a small change of the Rx position may result a large difference in the received power level even in the presence of line-of-sight between the Tx and Rx. It is found that the STD of received power level across the room increases with the decrease in HPBW of the antenna. As can be expected, directed antennas offer lower value of RMS-DS and RMS-AS compared with isotropic antenna.

Keywords: Channel characterization, 60 GHz, Measurements, Ray tracing, Simulations, Indoor radio channel, Delay spread, Angular spread

1 Introduction

Mobile communication technology is evolving at an accelerated pace due to widely growing usage of wireless devices over the past years. The development of fifth-generation (5G) enhanced mobile broadband (eMBB) services require higher capacity and data rates. Traditional mobile communication systems operating below 6 GHz frequency band are no longer fully able to satisfy the demand for extremely high user date rates and network capacity. Yet, the large frequency spectrum available at millimeter wave (mmWave) frequencies represents a potential solution to attain Gbps user data rate and multi-giga bytes (GBs) of cell capacity [1, 2].

The frequency spectrum around 60 GHz has been considered as a good candidate for 5G since the large available bandwidth provides a promising solution to fulfill the high data rate and high capacity requirements. On one hand, there are certain challenges associated with 60 GHz propagation, i.e., higher propagation and penetration loss, higher atmospheric absorption and rain attenuation, higher blockage loss induced by the people. Whereas, on the other hand, the small wavelength at 60 GHz facilitates the integration of large number of antenna elements and makes it more feasible to use directive antenna arrays at the transmitter and receiver end to perform beamforming [3, 4]. It is widely acknowledged that the 60 GHz band is suitable for short-range communication, i.e., for deploying wireless local and personal area network (WLAN/WPAN), and for indoor scenarios [5, 6]. In addition, large integrated antenna arrays with closely space elements become feasible at 60 GHz due to short wavelength [4]. Adding more number of antennas means more power is required, and it increases with the increase in the number of antennas.

While channel measurements provide a good insight to the indoor signal propagation at mmWave frequencies, the use of measurements in the wireless system performance evaluation is limited due to practical reasons: they are time consuming, complex and costly. In contrary, carefully executed simulations represent easier and more flexible option. In order to plan and design an efficient communication network operating at 60 GHz, accurate radio channel characterization and coverage prediction methodology are required [7]. In that task, the deterministic channel models, e.g., ray tracing (RT) models, are valuable since they are able to properly characterize the propagation phenomena. Here, accurate channel modeling requires information about the physical properties of the objects as well as a detailed geometrical plan of the environment [8].

Deterministic ray tracing models are valuable since they can be flexibly used to characterize the propagation phenomena. Descriptions of some RT and ray launching approaches can be found, e.g., from [8–10]. Actually, RT accurately describes multipath effects provided that radio environment and deployment configuration are well modeled. As such, RT has been applied in indoor and urban environments from early 1990s but interest toward RT simulation platforms has recently got increased as they provide more realistic results than stochastic models at mmWave frequencies. Also, the improved availability of computational resources in research organizations has supported the development. Besides accurate modeling, RT admits a notable advantage: it

is much less dependent on the bandwidth and carrier frequency than stochastic models those are based on measurements. Therefore, RT can be used with minor modifications to propagation simulations spanning from sub-6 GHz up to THz frequencies. Relevant and recent surveys on the topic can be found from [11, 12].

There are some recent studies on indoor mmWave channel modeling. In [13], authors modeled the 60 GHz indoor channel by shoot and bouncing ray (SBR) method and compared the small-scale properties of the channel with the measurements performed using a uniform virtual array. In [14], authors evaluated the accuracy of the simulations by comparing different channel properties like path loss, root mean square delay spread (RMS-DS), power delay profile (PDP) and spatial fading characteristics with the measurements. In [15], authors computed the PDP using a RT tool and modeled the diffuse scattering propagation mechanism by employing the directive model. Furthermore, in references [16, 17], authors investigated and validated the results of the RT simulations based on image theory with the measurement data in an outdoor microcellular and courtyard environment at 15 GHz, 28 GHz and 60 GHz and provided PDP and power angular spectrum (PAS) for different locations. In [18], authors examined the influence of the geometry on the clustering phenomenon at 60 GHz by applying a RT tool. Similar to the previous studies [13–20], in this paper we highlight the importance of using a RT tool in acquiring the channel responses in the direct orientation at 60 GHz.

In this article, the authors extended their work about the impact of type and position of the Tx and Rx antenna on the characteristics of channel at 60 GHz frequency in a conference room [21]. At first, the simulation results acquired with the in-house built RT tool are validated with the measurement data provided in [22]. In the second part of this research work, the main target is to study about the variation in the characteristics of the channel, i.e., received power, RMS-DS and root mean square angular spread (RMS-AS) in azimuth plane, while the receiver position is shifted by a small distance of around 20 cm. For this purpose, we have considered a grid of 3×3 points at each receiver location with a separation of 20 cm. This study highlights the impact of error that is made while estimating the position of the receiver for simulations. Different configurations of the Tx and Rx antennas are compared and investigated through 3D RT simulations, and in the last part of this research work, the impact of utilizing different antenna half power beamwidth (HPBW) at the Tx side is studied.

The rest of the paper is organized as follows. The measurement setup and measurement scenario are described in Sect. 2. The details of the simulation methodology, setup and simulation tool are described in Sect. 3. Section 4 presents a comparison between the measurement and the simulation results and provides discussion about acquired results. Finally, Sect. 5 concludes the paper.

2 Measurement setup and scenario

2.1 Measurement setup

Figure 1 shows the detailed block diagram of the measurement setup and highlights the function of each element. The measurement setup consists of different elements, e.g., vector network analyzer (VNA) operating at the center frequency of 3.5 GHz, multipliers and mixers for up and down conversion of signals, 70 MHz oscillator, 18.83 GHz phase locked oscillator (PLO), filters and antennas. The function of the VNA is to measure the

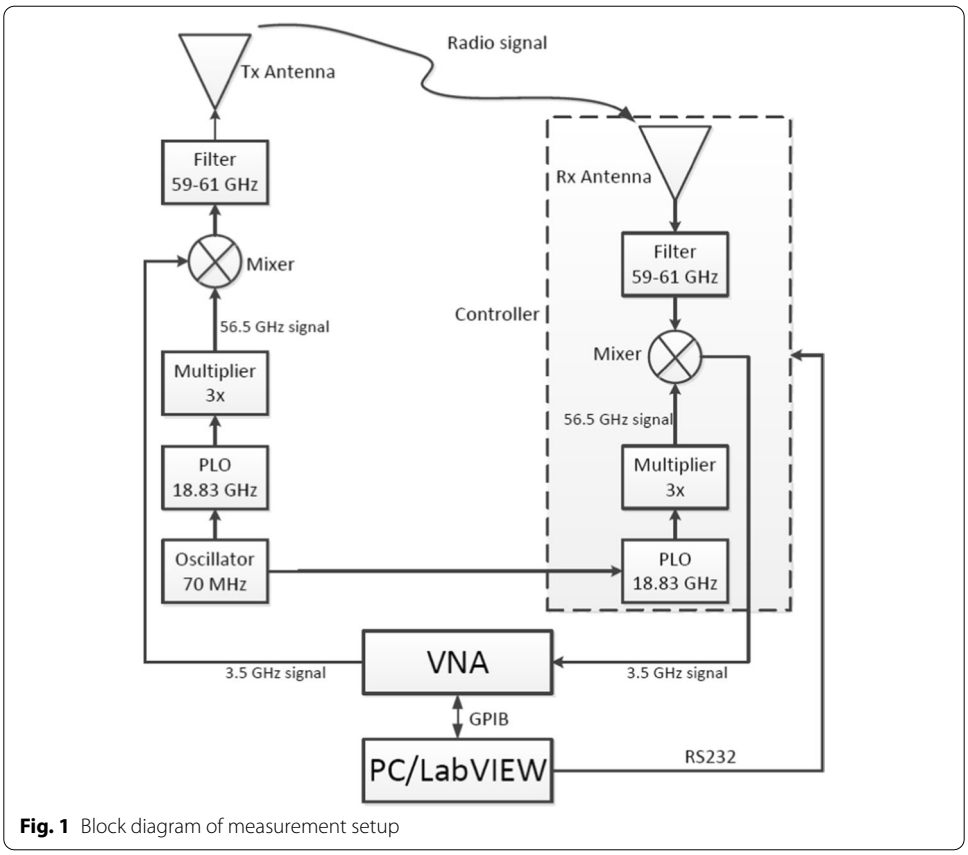

Fig. 1 Block diagram of measurement setup

magnitude and phase of the S_{21} parameter over 2 GHz bandwidth, i.e., at 401 equidistant carriers with a step of 5 MHz. The frequency band of the measurement system is 59–61 GHz with a centre frequency of 60 GHz. Measurements were conducted with two types of antennas for the transmitter (Tx), i.e., an omnidirectional antenna (SAGE Millimeter 5836230230-15-S1) in the horizontal/azimuth plane and 30° half power beamwidth (HPBW) in the vertical/elevation plane, and the other type of antenna used at the Tx is a vertically polarized horn antenna with 100° HPBW in both horizontal (H) and vertical (H) planes. The maximum antenna gain for omnidirectional and horn antenna used at the Tx is 2 dBi and 7.3 dBi, respectively, while the receiver is equipped with narrow beamwidth horn antenna and has 10° and 13° HPBW in vertical and horizontal plane, respectively. The Rx antenna has a maximum antenna gain of 22.5 dBi. The narrow beam Rx antenna provides good spatial resolution and that helps in capturing the angle of arrival of the multipaths. The radiation patterns of the antennas utilized in the measurements and simulations are shown in Fig. 2. These antenna radiation patterns are supplied by the antenna manufacturers in their data sheets. The Rx and Tx are connected to VNA through coaxial cables of length 1 m and 20 m, respectively. A full two-port calibration was performed to compensate the cable losses. The transmission power is set to 0 dBm. The receiver antenna is placed on the positioner/motor, and the direction of the Rx antenna is set by the PC installed with LabVIEW program. The PC sends a command to the positioner via RS232 cable. Finally, the measurement data are collected at PC and that are connected to VNA via a GPIB cable.

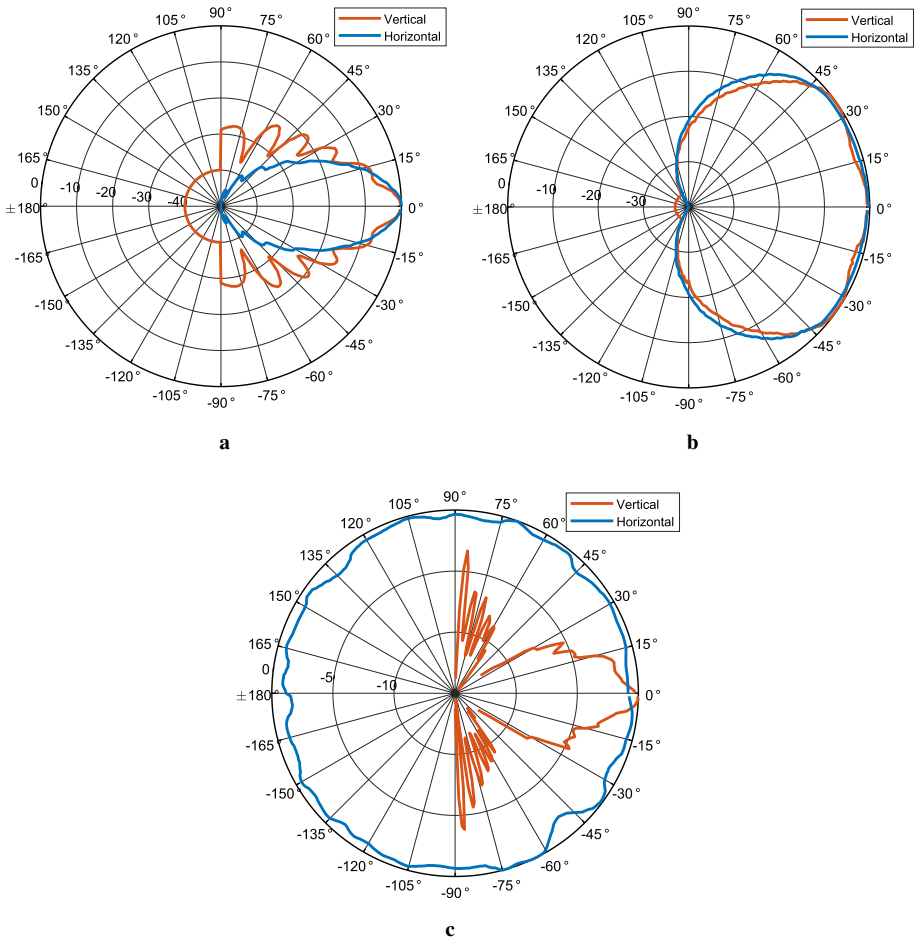

Fig. 2 Antenna radiation patterns, **a** Antenna with 10° and 13° HPBW in V and H-plane, respectively, **b** antenna with 100° HPBW in both V and H-plane, and **c** omnidirectional antenna with 30° and 360° HPBW in V and H-plane, respectively

2.2 Measurement scenario

Measurements were conducted in a typical conference room of dimension 6.6 × 3.2 m, having a central conference table and ten chairs around the table. It is critical to highlight here that measurements were performed in the absence of the people, and hence, the impact of human obstruction is not considered. The conference room is equipped with two white boards on the walls, and there is a big glass window on one side of the room as highlighted in Fig. 3. In order to provide best possible coverage in the room, the enigma is to optimally locate the Tx antenna and to select the type of the antenna. The measurements were realized for two different positions and configurations of the Tx antenna, as stated here:

Tx1-Config1 In this configuration, the measurement scenario depicts an event of the conference where an omnidirectional antenna in the horizontal plane is placed at the center of the conference table at the height of 1.2 m with respect to the ground as highlighted by Tx1 and red filled circle in Fig. 3. The positions of the sitting users

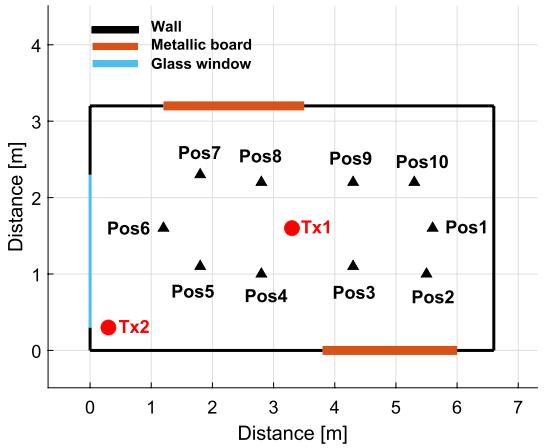

Fig. 3 Illustration of conference room with Tx and Rx positions

around the table with their wireless equipment at 1 m height are highlighted with triangles in Fig. 3.

Tx2-Config1 In the second configuration, a directed horn antenna is raised to the height of 1.9 m above the ground and is placed in the bottom-left corner of the room as indicated by red filled circle and text Tx2 in Fig. 3. The main beam of the Tx2 antenna was pointing in the direction of the up-right corner of the room.

3 Simulation methodology

The first target of this study is to compare and validate the RT simulation results with the measurement results. Therefore, at first the measurement cases discussed in Sect. 2.2 are simulated while utilizing an in-house built 3D RT tool in MATLAB. The ray tracing simulations are generally used to exploit the spatial characteristics of the environment and that helps in better understanding the radio channel response. The deterministic approach of RT utilizes the geometry of the environment, and the location of the Tx and Rx for finding different propagation paths. Our RT tool works on the principle of Image Theory (IT), presented in [8]. The radio environment and the objects present in the radio environment is modeled with the help of multiple lines as shown in Fig. 3. In case of IT method, for finding a propagation path with single reflection, a mirror image of the Tx is created with respect to each line of the radio environment model. For next order reflection, the next level images are created and so on. Whereas, for diffracted paths, each corner of the object acts as a source point. Ray tracing tool finds the LoS path along with other propagation paths between the Tx and the Rx with the given number of interactions, i.e., reflections, diffractions and a mix of reflections and diffractions. As a result of adequately high penetration/transmission loss through the materials at 60 GHz, the penetrated paths through the obstacles and walls are not considered in the simulations. We have only considered the ray paths with two reflections and one diffraction at maximum. Each path has certain amplitude, delay and phase. Antenna radiation patterns shown in Fig. 2 are used for antenna masking over ray tracing data to include the impact of the antennas at the Tx and Rx end. Other general parameters, e.g., antenna heights,

transmission power, frequency of operation, azimuth and downtilt of the Tx and Rx antennas are set in the simulations as were used in measurements. Figure 4a, b illustrates the propagation paths obtained through ray tracing simulations for receiver position 10 with Tx1-Config1 and Tx2-Config1, respectively.

In the second part of this study, we extended our 3D RT simulations in two ways. Initially, from the measurement scenarios the exact position of the receiver points was extracted, and simulations were done only for those positions. Later, we created a grid of test positions around the actual receiver position as shown in Fig. 5, in order to investigate the change in channel characteristics while the receiver position is altered by a small distance of just 20 cm. In Fig. 5, the red circle represents the position of the receiver used during the measurement, while the green circles represent the position of extra test points around the original position of the receiver.

Next, we have considered two more special antenna configurations for simulations, as stated here:

Tx1-Config2 In this configuration, same Tx antenna position is used as in TX1-Config1. However, an ideal isotropic antenna with 0 dBi gain and perfect circular antenna

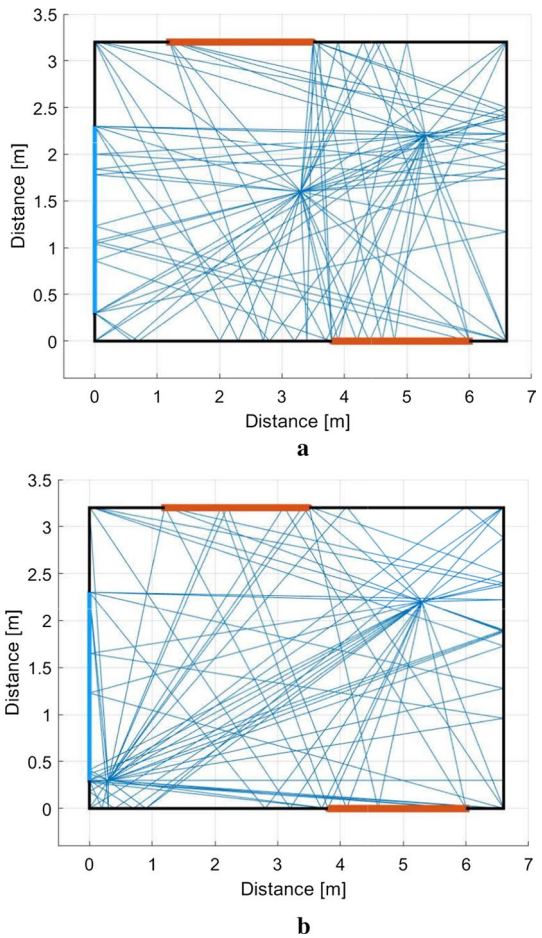

Fig. 4 Propagation paths obtained through ray tracing for position 10 with, **a** Tx1, and **b** Tx2

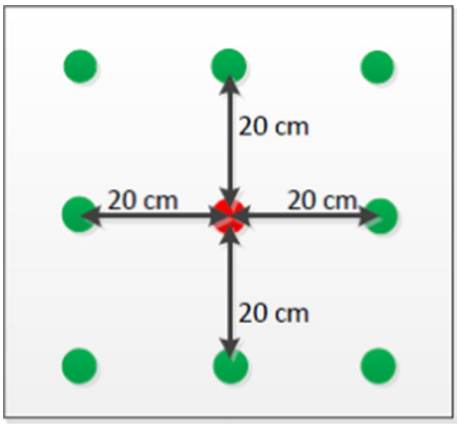

Fig. 5 A 3 × 3 grid of receiver points

radiation pattern in both horizontal and vertical domain is considered at Tx and Rx end. Hence, in this way the impact of only radio channel can be analyzed, independent of the antenna type used at the Tx and Rx.

Tx2-Config2 Similarly, in this case same Tx antenna location is used as in TX2-Config1, but isotropic antenna is used at the Tx and Rx side. The measurement data for Tx1-Config2 and Tx2-Config2 are not available.

Finally, we have investigated the impact of Tx antenna HPBW on different considered channel characteristics. In case of Tx1, the antenna is placed in the centre of the conference room, therefore, it is not feasible to use a directional antenna for Tx1. Whereas, in case of Tx2, the antenna is located in the corner of the room, therefore, we studied the impact of antenna HPBW for Tx2 only. For this purpose, we have considered five different horn antennas with 100°, 44°, 29°, 16.5° and 10° HPBW in both H and V-plane. The radiation pattern of the 100° HPBW antenna is shown in Fig. 2b, whereas, radiation patterns of other horn antennas are shown in Fig. 6. The maximum antenna gain is 7.3, 10, 15, 20, and 25 dBi for antenna with 100°, 44°, 29°, 16.5° and 10° HPBW, respectively. These antenna radiation patterns of horn antennas are supplied by the antenna manufacturer, and other technical specification can be found in their data sheets given at [23].

4 Results and discussion

This section discusses about acquired results and shows a comparison between the measurement and simulation results. Figure 7 shows the received power levels at various receiver positions with different Tx–Rx configurations, where the x-axis shows the position number of the Rx, and the y-axis is the received power in dBm. In Fig. 7a, b, blue line shows the measured received power levels, black solid line indicates the simulated received power levels at absolute receiver positions, the red dots represent the received power levels at those extra test points around the actual position of the receiver, and black dashed line shows the mean received power of nine test positions. It is important to highlight here that for Tx1-Config1 and Tx2-Config1 cases the results are reported with DO, that means the antenna of the receiver was oriented in the direction of the strongest incoming path. Now, it is fascinating to see

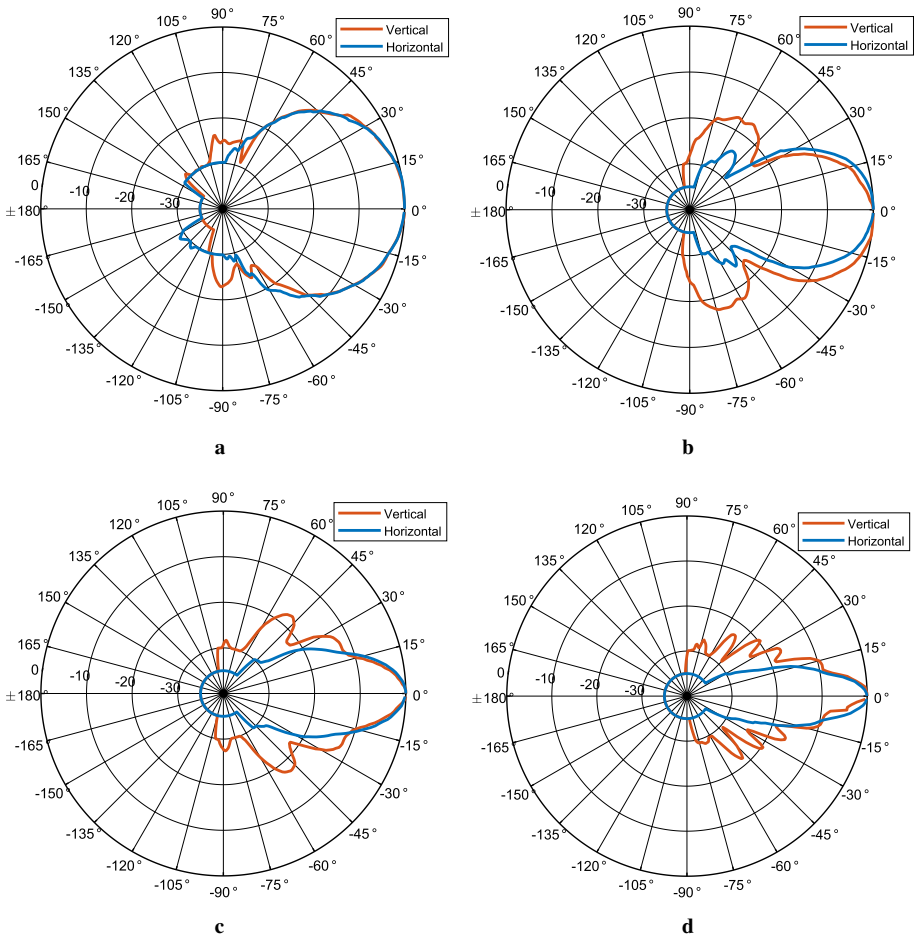

Fig. 6 Antenna radiation patterns. **a** Antenna with 44° HPBW in both V and H-plane, **b** antenna with 29° HPBW in both V and H-plane, **c** antenna with 16.5° HPBW in both V and H-plane and **d** antenna with 10° HPBW in both V and H-plane

that a remarkable good match is found between the measured and simulated received power levels for both Tx1-Config1 and Tx2-Config1 for all ten Rx positions. The RMS error between the measured and simulated received power level is around 2.6 dB and 2.9 dB in case of Tx1-Config1 and Tx2-Config1, respectively. It highlights the ability of ray tracing simulations done with in-house built RT tool to predict the received power with quite good accuracy level. Figure 7a, b shows that due to high directive gain of the Rx antenna and with small Tx antenna gain the received power levels were adequately high, and it is learned from the RT simulation results that the average received power of ten receiver positions is around −45 dBm and −59.3 dBm for Tx1-Config1 and Tx2-Config1, respectively. Furthermore, it can be seen in Fig. 7a, b that even in a static environment the received power level fluctuates significantly due to constructive and destructive addition of multipaths, while the receiver position is shifted by a small margin of just 20 cm. The average standard deviation (STD) of signal variation caused by the displacement of Rx position at eight different positions around the central position in grid is around 6.5 dB in both Tx1-Config1 and Tx2-Config1. Interestingly, the mean of nine points grid is again found in close harmony

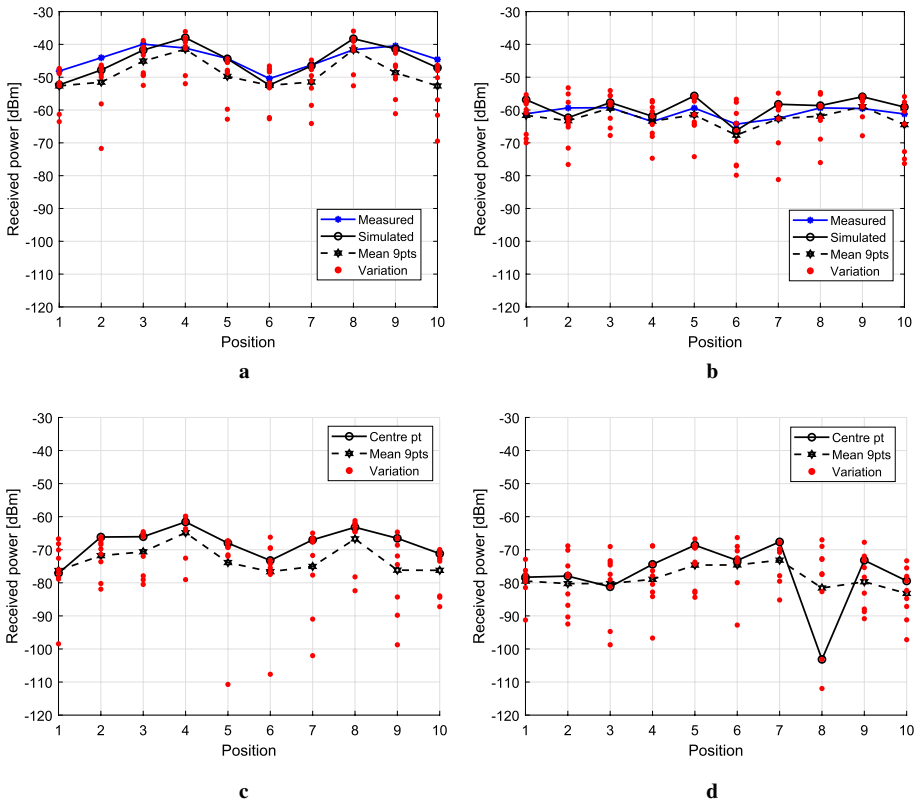

Fig. 7 Received power at receiver positions with, **a** Tx1-Config1, **b** Tx2-Config1, **c** Tx1-Config2 and **d** Tx2-Config2

with the measured received power level of the central point. Whereas, the RMS error between the measured value and the mean of nine points is around 5.4 dB and 2.2 dB for Tx1-Config1 and Tx2-Config1 configurations, respectively. Hence, it shows that in the absence of exact information about the receiver location, it is more beneficial to consider a mean of multiple nearby locations in order to minimize the coverage prediction error with RT simulations.

Figure 7c, d presents the received power levels for the configurations with ideal isotropic antennas at the Tx and Rx, i.e., for Tx1-Config2 and Tx2-Config2, respectively. Ideal isotropic antenna does not filter the multipaths in spatial domain. The solid black line shows the result of central location of the receiver grid, and black dashed line represents the mean of nine points of the grid. The received power levels shown in Fig. 7c, d are significantly lower, and the average STD is around 9.5 dB and 8.5 dB with Tx1-Config2 and Tx2-Config2, respectively. It can be seen that the signal level fluctuates more in case of isotropic antennas, and there were few samples with below − 100 dBm. Remember, we have only considered a LoS scenario in our simulations, while the signal levels would be much lower in case of obstructed or non-LoS. Again, the results presented in Fig. 7c, d indicate that it is better to consider the mean of several near by points while estimating the received power levels, otherwise RT simulation results may lead to either highly optimistic or pessimistic outcome due to

varying nature of the signal at 60 GHz. One of its example can be seen in Fig. 7d that at receiver position 8, the received power level at central point is − 102 dBm whereas the mean value of 9 points is around − 81 dBm.

We have investigated the power delay profile (PDP) and power angular profile (PAP) through RT simulations at each receiver position with respect to four different considered Tx–Rx configurations, in the direction of DO. However, here we are discussing only the PDP and PAP at Pos 3 in detail. Figure 8a, b shows the PDP of Pos 3 for different configurations of Tx1 and Tx2 antennas, respectively, where the x-axis is time in ns, and the y-axis is the normalized power in dB. The power for each configuration is separately normalized with respect to the strongest in coming path, i.e., a direct LoS path in our case. Although, we have considered a large dynamic range of 60 dB power for showing the multipaths in PDP; however, major contribution is coming from the path within 20–25 dB range [7]. Figure 8c, d shows the PAP in azimuth plane at the receiver Pos 3 for different configurations of Tx1 and Tx2, respectively, where the x-axis is the direction of arrival (DoA) in horizontal plane of incoming paths at the Rx end in degrees, and the y-axis is the normalized power. The right side of the Rx corresponds to 0° of DoA. In order to better understand the temporal characteristics of the channel, both PDP and PAP are discussed together. In Fig. 8a, it can be seen that in case of configuration with directed antenna at the Tx and Rx, i.e.,

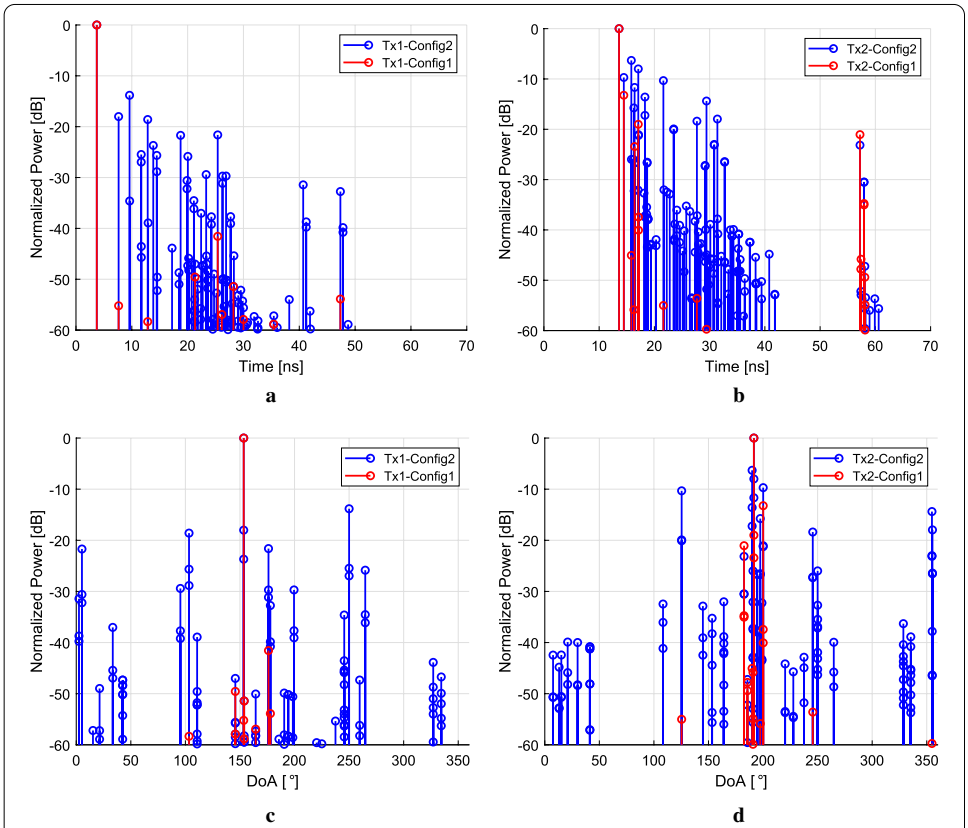

Fig. 8 Channel characteristics at Pos 3. **a** PDP with Tx1 configurations, **b** PDP with Tx2 configurations, **c** PAP with Tx1 configurations and **d** PAP with Tx2 configurations

Tx1-Config1 (red line), major share of the received power is coming with a delay of 3.7 ns, and that corresponds to a path length of 1.1 m. In Fig. 8b, it can be seen that strongest path has a DoA = 153° and this coincides with the actual measurement/simulation environment. As a result of directive Tx–Rx antennas, rest of the multipaths are spatially filtered out. However, in case of isotropic-isotropic configuration, i.e., Tx1-Config2 (blue lines), a large number of multipaths can be seen in Fig. 8a, c. The second strongest path is the reflected path from the nearby wall of Pos 3, and the strength of reflected path is 13.8 dB less as compared to the strongest path, and it arrives with a delay of 9.6 ns, and that corresponds to the path length of 2.88 m and has a DoA = 250°. With these results, one should expect a smaller value of delay spread and angular spread in case Tx1-Config1, whereas it is clearly evident in Fig. 8a, c that the Tx1-Config2 has large DS and AS due to wide spread PDP and PAP.

Similarly, in Fig. 8b, d it can be seen that in case of Tx2, the strongest path arrives with a delay of 13.6 ns that corresponds to the path length of 4.1 m with DoA = 192°. The PDP of Tx2-Config2 presented in Fig. 8b shows that it is highly multipath rich environment. However, narrow HPBW antennas filter most of the multipath in spatial domain and hence only few paths are left with significant power with directive antennas. With Tx2-Config1, the second strongest path is the first-order reflected path from the nearby wall on the right side of the Tx2, and that reflected path arrives almost together with the strongest path. The power of the first-order reflected path is about 13.2 dB lower than the direct path and has a delay of 14.5 ns which corresponds to the path length of 4.35 m with DoA = 200°. There is another second-order reflected path that arrives with a delay on 57 ns, and the power of the second reflected path is around 21 dB lower with reference to strongest path. The PDP and PAP of nine positions with respect to all considered Tx–Rx configurations are shown in "Appendix".

In radio propagation, the most commonly used parameter to characterize the time domain dispersion of the radio channel is the RMS-DS [5, 24], and it has a high dependence on the HPBW of the applied antennas. Figure 9 shows the root mean square delay spread for ten receiver positions with different configurations. It was found while comparing Figs. 7 and 9 that for any particular Tx position in LoS condition, there exists a relationship between the received power level and delay spread, and RMS-DS is found inversely proportional to the received power level. The simulation results revealed that the receiver positions with higher received power have lower RMS delay spread, and vice versa. Again, the average value of 9 points grid seems to be a safer choice for estimating the RMS-DS of channel, as RMS-DS was also found varying with minor Rx displacement. Secondly, as mentioned earlier while discussing the PDP of Pos 3 that it is intuitive that directional antennas provide smaller values of RMS-DS than wide beam antennas. Considering average value of 9 points grid at each receiver position, the mean value of DS is 1.1 ns and 4 ns for Tx1-Config1 and Tx1-Config2, respectively. Similarly, for Tx2-Config1 and Tx2-Config2 the mean value of RMS-DS in the room is 3.2 ns and 4.3 ns, respectively. In Fig. 9b, there are few samples of RMS-DS with values greater than 10 ns. In case of isotropic antennas, RMS-DS value depends on the room size and on the reflective properties of the material and walls of the environment. It is learned from these results that RMS-DS can be significantly reduced by employing high gain directive antennas, and in turn increases the coherence bandwidth of the channel.

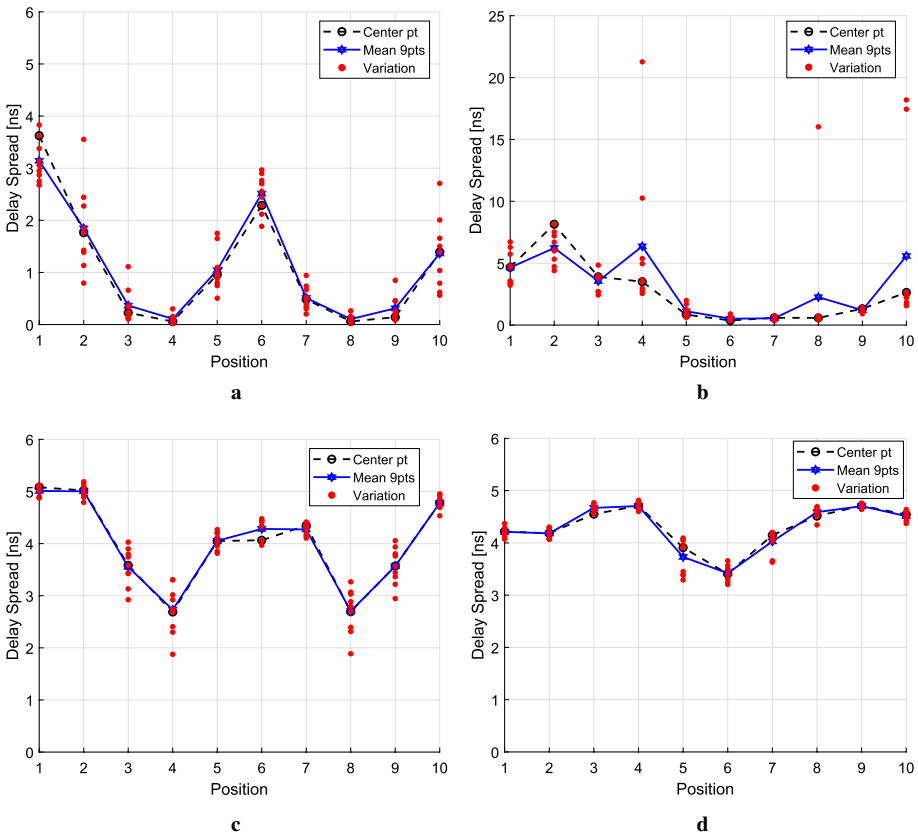

Fig. 9 Root mean square delay spread at ten receiver positions with **a** Tx1-Config1, **b** Tx2-Config1, **c** Tx1-Config2 and **d** Tx2-Config2

Figure 10 shows the result of RMS-AS in azimuth plane at receiver positions. The RMS-AS is computed similar to RMS-DS, where the factor delay spread is replaced with angular spread as given in reference [24]. The configurations with directive antennas clearly have a narrow angular spread compared with the configuration with isotropic antennas at the Tx and Rx. Obviously, an isotropic antenna has a better capability to collect the energy coming from all directions than a directed beam antenna. However, in case of directional antennas the beams of the Tx and Rx antennas should be properly aligned in order to capture maximum energy. It can be seen in Fig. 10a that for Tx1-Config1 the angular spread in azimuth plane does not vary much while the receiver position is shifted by a distance of 20 cm around the central point. Whereas, few points with large variations are observed with Tx2-Config1 in Fig. 10b. However, a comparatively larger variation in RMS-AS can be found for isotropic-isotropic Tx–Rx configuration while the Tx antenna is placed in the middle of the conference room, i.e., Tx1-Config1. The mean value of RMS-AS in the room is 0.4° and 1.4° for Tx1-Config1 and Tx1-Config2, respectively, whereas the average value of AS is 32.0° and 32.8° for Tx1-Config2 and Tx2-Config2, respectively. Finally, Table 1 shows the summary of simulation results acquired through 3×3 grid points at each receiver location for different Tx–Rx configurations.

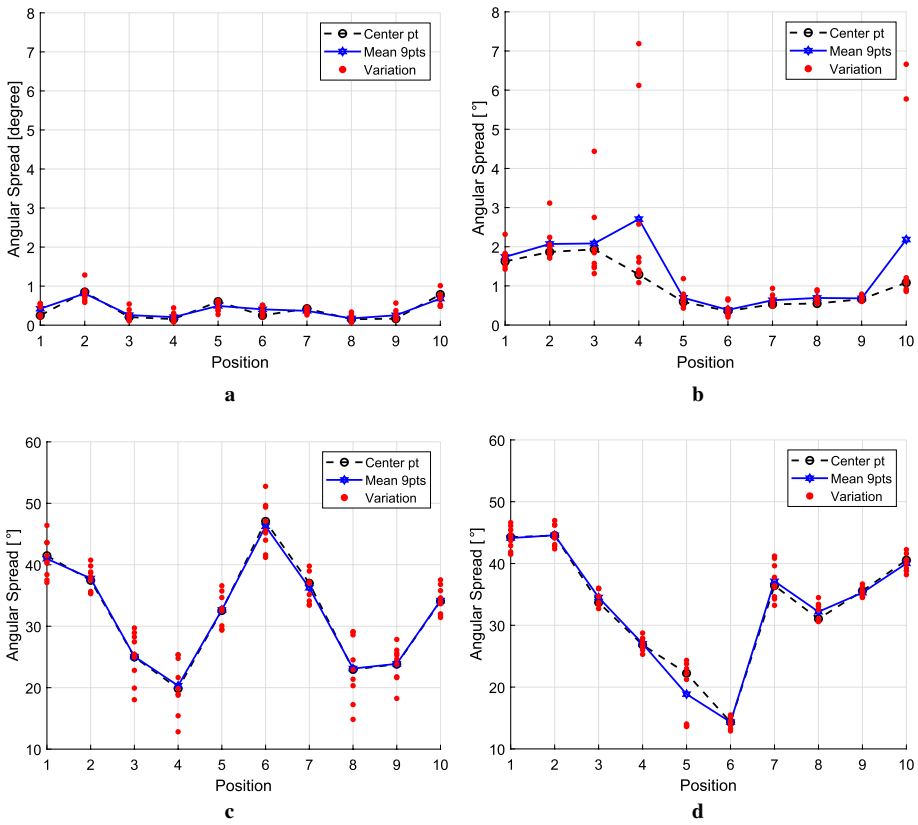

Fig. 10 Angular spread at receiver positions with, **a** Tx1-Config1, **b** Tx2-Config1, **c** Tx1-Config2 and **d** Tx2-Config2

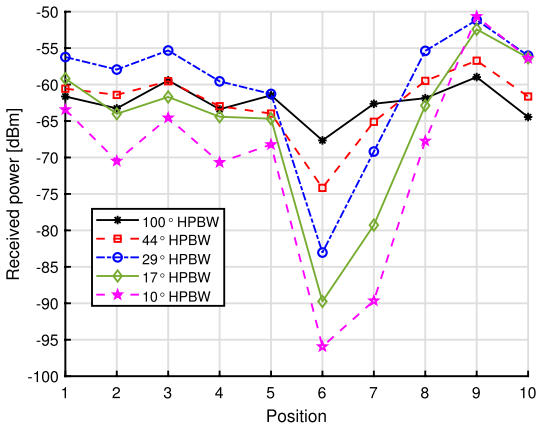

Fig. 11 Received power at receiver positions with different Tx2 antenna HPBWs

In the last part of this study, we have investigated the impact of antenna HPBW on channel characteristics. Figure 11 shows the mean received power of grid points for ten receiver locations, acquired through different antenna types at Tx2 position. For better understanding the received power results presented in Fig. 11, the Tx and receiver positions shown in Fig. 3 should be kept in mind. It can be seen in Fig. 11 that 100° HPBW

antenna provides almost homogeneous coverage in the room due to wide beamwidth of the antenna; however, the overall received signal power was improved with 29° HPBW antenna compared with 100° HPBW antenna except for receiver positions 6 and 7. Secondly, it can also be seen that the STD of the received signal level across the receiver positions increases with the decrease in HPBW of the antenna. It must be noted that position 6 is badly impacted by using narrow antenna, as position 6 is located off the main beam direction. It is interesting to see that although 17° and 10° HPBW antennas have higher gain compared with other considered antennas, yet due to narrow HPBW the received power level of all positions except positions 9 and 10 is inferior compared with other antennas. Interestingly, the acquired results of received power show that 44° and 29° HPBW antennas are a good choice for providing adequate coverage in a conference room.

Figure 12 shows the average RMS-DS of grid points for ten receiver locations. It should be noted that positions 9 and 10 lie close to the main beam of the Tx antenna, and at those positions the RMS-DS is the direct function of the antenna HPBW, i.e., narrow the HPBW of the antenna the smaller is the RMS-DS. However, the same trend is not valid for all the positions in the room, as in case of other positions they are off the main beam. Again, with narrow HPBW antennas, i.e., 17° and 10°, the value of RMS-DS at position 6 is quite high compared with other positions. The results presented in Fig. 12 reveal that 29° HPBW antenna provides comparatively better, i.e., lower values of RMS-DS, and lower STD than other antennas.

Finally, Fig. 13 shows the average RMS-AS of grid points for ten receiver locations. It can be seen in Fig. 13 that 44° and 29° HPBW antennas provide low angular spread in azimuth plane compared with other antennas, and the average value of RMS-AS is 1.4°, 1° and 0.9° is obtained with 44° and 29° HPBW antenna, respectively. Similarly, the STD of RMS-AS across 10 receiver positions is 0.8°, 0.6° and 0.8° with 100°, 44° and 29° HPBW antenna, respectively.

Finally, the summary of simulation results acquired through 3×3 grid points at each receiver location is presented in Table 1. The first column shows the transmitter position, the second and third columns show the HPBW of the antenna in both V and H

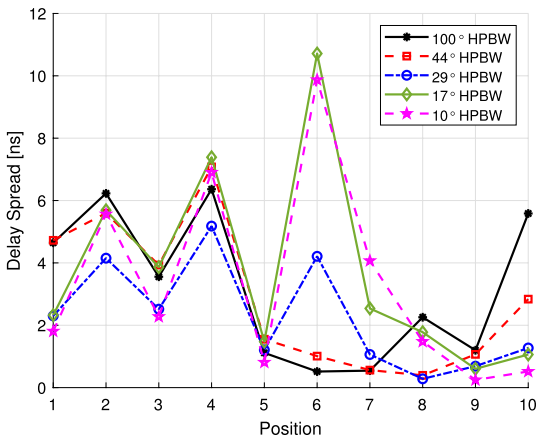

Fig. 12 Root mean square delay spread at receiver positions with different antenna HPBWs

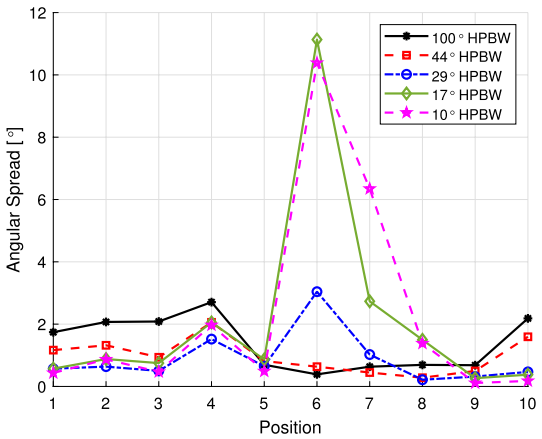

Fig. 13 Root mean square angular spread at receiver positions with different antenna HPBWs

plane at the Tx and Rx side, respectively. Next two columns show the mean and the STD of received power level considering ten receiver locations, and the sixth column shows the average STD of received signal across the points within the 3 × 3 grid. Similarly, the seventh and eighth columns show the average and the STD of RMS-DS considering ten receiver locations, and the ninth column shows the average STD of RMS-DS across the points within the 3 × 3 grid. Similarly, the statistical results of RMS-AS are also presented in Table 1.

5 Conclusions

This article investigated the characteristics of the 60 GHz radio signal propagation in a typical conference room. The room dimensions were 6.6 × 3.2 m, and signal data were obtained through measurements and 3D RT simulations from ten different positions around the central table. In the first part of the work, we examined the impact of the location and type of the applied antenna on the radio channel in the LoS condition. In addition, we validated the acquired 3D RT simulation results against measurements by using two system configurations called as *Tx1-Config1* and *Tx2-Config1*. The received power RMS error was only 2.6 dB and 2.9 dB between the measured and simulated results for *Tx1-Config1* and *Tx2-Config1*, respectively. In the second part of the work, we investigated the channel characteristics using simulations only. We carried out the simulations such that the Rx was shifted step-by-step by around 20 cm to eight different positions around the central position to obtain a uniform grid of 3 × 3 Rx points. In addition, we investigated several Tx–Rx configurations with directed antennas of different HPBW, omnidirectional antenna and isotropic antenna. As performance indicators, we considered receiver power level, power delay profile, power angular profile, RMS delay spread and RMS angular spread in azimuth plane, assuming the Rx antenna is directly oriented in the direction of the Tx. Interestingly, we found that even with LoS a slight displacement of Rx by 20 cm causes an average STD of around 6.5 dB in the received power level in case of directed antennas. With isotropic antennas such displacement leads up to 9.5 dB STD. However, the average received power over nine points in a grid (nearby Rx locations) was found to be in

Table 1 Summary of simulation results acquired through 3 × 3 grid points at each receiver location

	Tx antenna HPBW V/H (°)	Rx antenna HPBW V/H (°)	Mean Rx level (dBm)	STD of Rx level (dB)	Avg STD of Rx level in grid (dB)	Avg RMS-DS (ns)	STD of RMS-DS (ns)	Avg STD of RMS-DS in grid (ns)	Avg RMS-AS (°)	STD of RMS-AS (°)	Avg STD of RMS-AS in grid (°)
Tx1	30/360	10/13	− 48.7	4.4	6.5	1.1	1.1	0.4	0.4	0.2	0.1
Tx1	Isotropic	Isotropic	− 72.8	4.2	9.5	4.0	0.8	0.3	32.0	8.6	3.3
Tx2	100/100	10/13	− 62.5	2.5	6.5	3.2	2.4	2.3	1.4	0.8	0.7
Tx2	44/44	10/13	− 62.6	4.7	7.3	2.9	2.3	1.7	1.0	0.6	0.6
Tx2	29/29	10/13	− 60.5	9.3	7.9	2.3	1.7	1.5	0.9	0.8	0.6
Tx2	16.5/16.5	10/13	− 65.5	11.0	7.8	3.7	3.3	2.6	2.1	3.3	1.8
Tx2	10/10	10/13	− 69.8	13.7	7.4	3.4	3.2	2.1	2.3	3.4	1.2
Tx2	Isotropic	Isotropic	− 78.6	3.3	8.5	4.3	0.4	0.1	32.8	10.1	1.8

a close harmony with the measured received power levels. Accordingly, we propose that in an absence of exact information about the Rx position for 60 GHz propagation simulations, a grid of 3×3 Rx points should be used instead of using single point values in order to minimize the received power prediction error.

The simulated PDP and PAP results demonstrate the strong relationship between the acquired RT multipaths and the propagation environment. Results show that in case of directed antennas and LoS the major signal power is coming through the LoS path and reflected paths within the main beam direction, while in case of isotropic antenna the signal energy is collected from all directions. While considering the average value over a 9-point grid within each receiver position, the obtained results show that the Tx antenna placed in the centre of the table provides lower RMS-DS as compared to the Tx antenna placed in the corner of the conference room. It was also found that the deployment of directed antennas at Tx and Rx lowers the RMS-DS. Furthermore, the RMS angular spread depends upon the HPBW of the applied antennas and, with directed antennas, the average RMS-AS in the room was found to be around 0.4° and 1.4° for *Tx1-Config1* and *Tx2-Config1* with 100° HPBW antenna, respectively, whereas the average value of AS is increased to 32.0° and 32.8° for *Tx1* and *Tx2* with isotropic antennas, respectively.

In the last part of this study, for the transmitter located in the corner of the conference room, the impact of antenna HPBW on different channel characteristics was investigated. The simulations were done with 100°, 44°, 29°, 16.5° and 10° HPBW antennas, and the obtained simulation results revealed that 100° HPBW antenna provides almost homogeneous coverage in the room, whereas 44° and 29° HPBW antennas are also a good choice in terms of offering adequate coverage in the conference room. The acquired simulation results show that the STD of received power level in the conference room increases with the decrease in HPBW of the Tx antenna. Interestingly, 29° HPBW antenna shows best performance among all considered antennas in terms of RMS-DS and RMS-AS.

In future, our aim is to extend this work and study the impact of minute displacement, i.e., 20 mm of the receiver position on different channel characteristics. In our current work, a grid of 3×3 Rx points was considered, whereas in our future work our target is to create a fine grid of 20×20 points with 20 mm separation between them. It will help us in better understanding the variation of signal level due to small and large scale fading.

Appendix

See Figs. 14, 15, 16, 17.

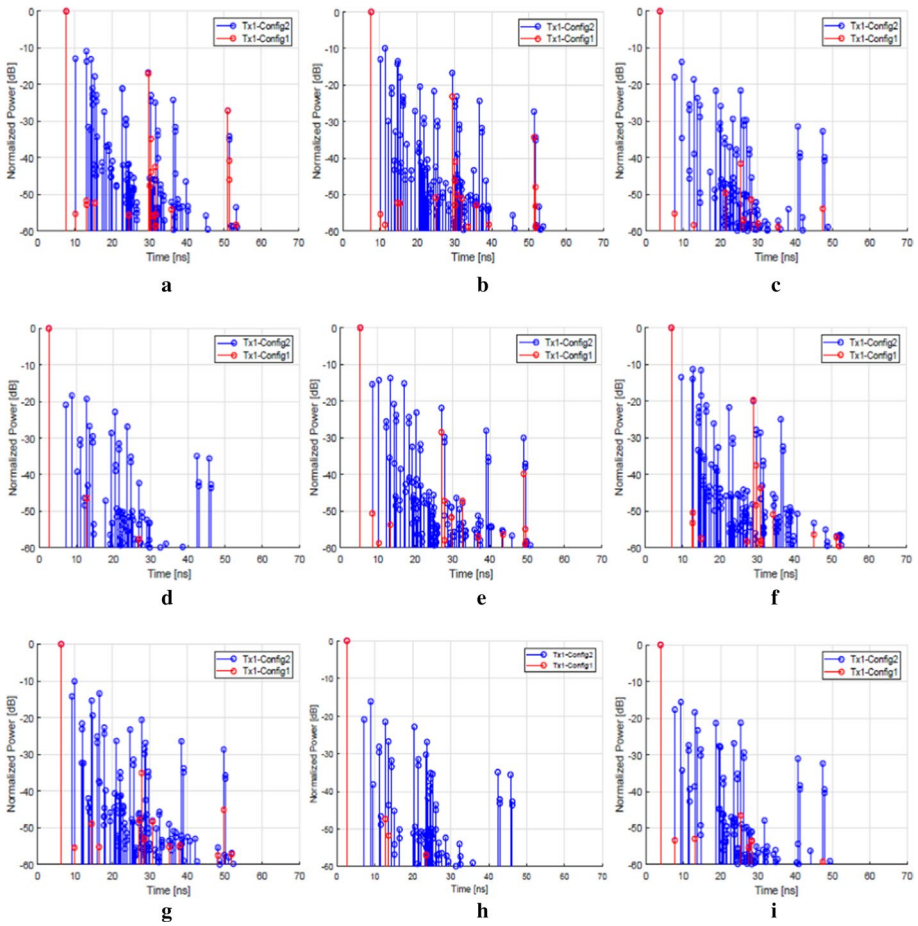

Fig. 14 Power delay profile. **a** Pos 1, **b** Pos 2, **c** Pos 3, **d** Pos 4, **e** Pos 5, **f** Pos 6, **g** Pos 7, **h** Pos 8, and **i** Pos 9

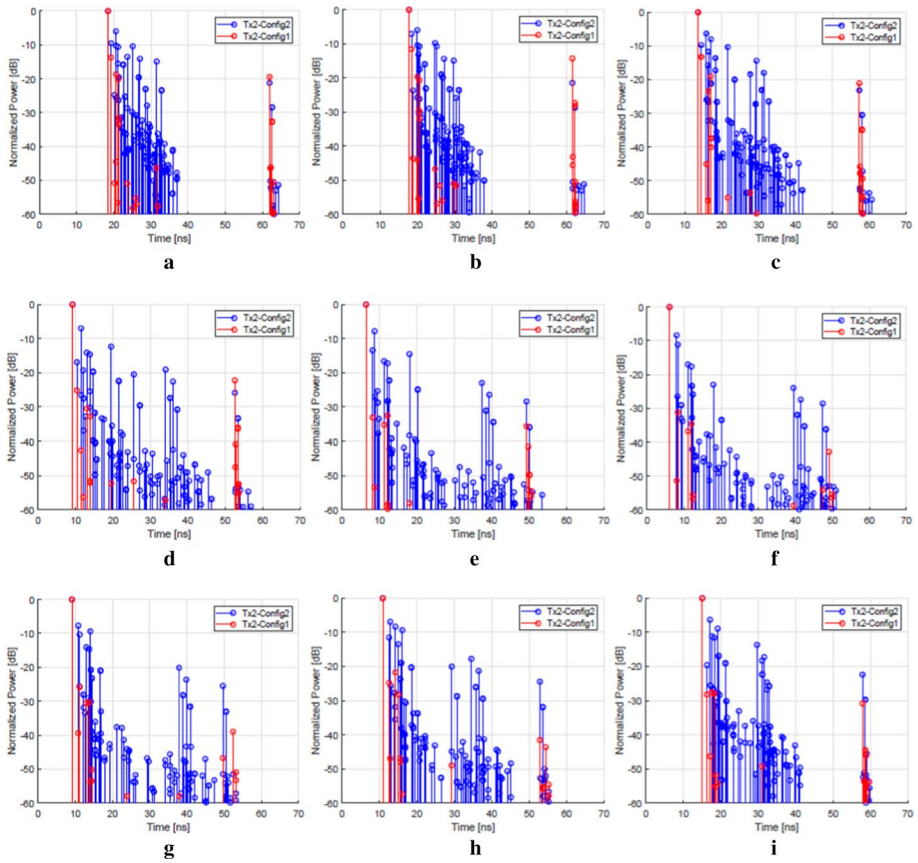

Fig. 15 Power delay profile with Tx2. **a** Pos 1, **b** Pos 2, **c** Pos 3, **d** Pos 4, **e** Pos 5, **f** Pos 6, **g** Pos 7, **h** Pos 8, and **i** Pos 9

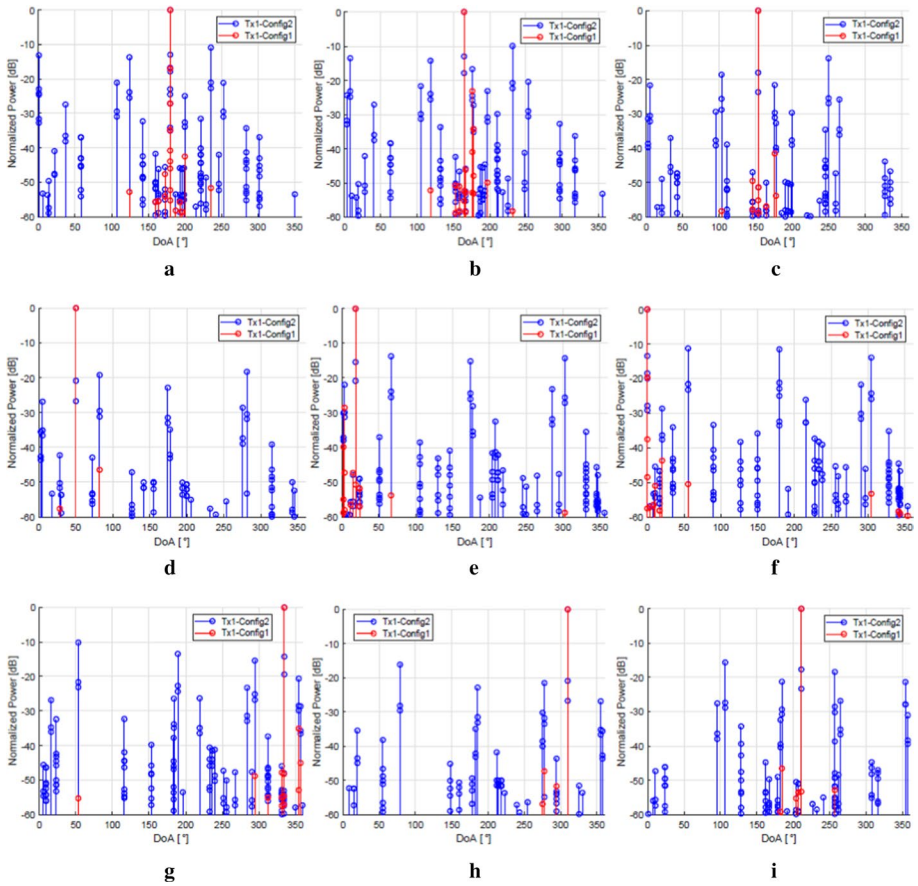

Fig. 16 Power angular profile. **a** Pos 1, **b** Pos 2, **c** Pos 3, **d** Pos 4, **e** Pos 5, **f** Pos 6, **g** Pos 7, **h** Pos 8, and **i** Pos 9

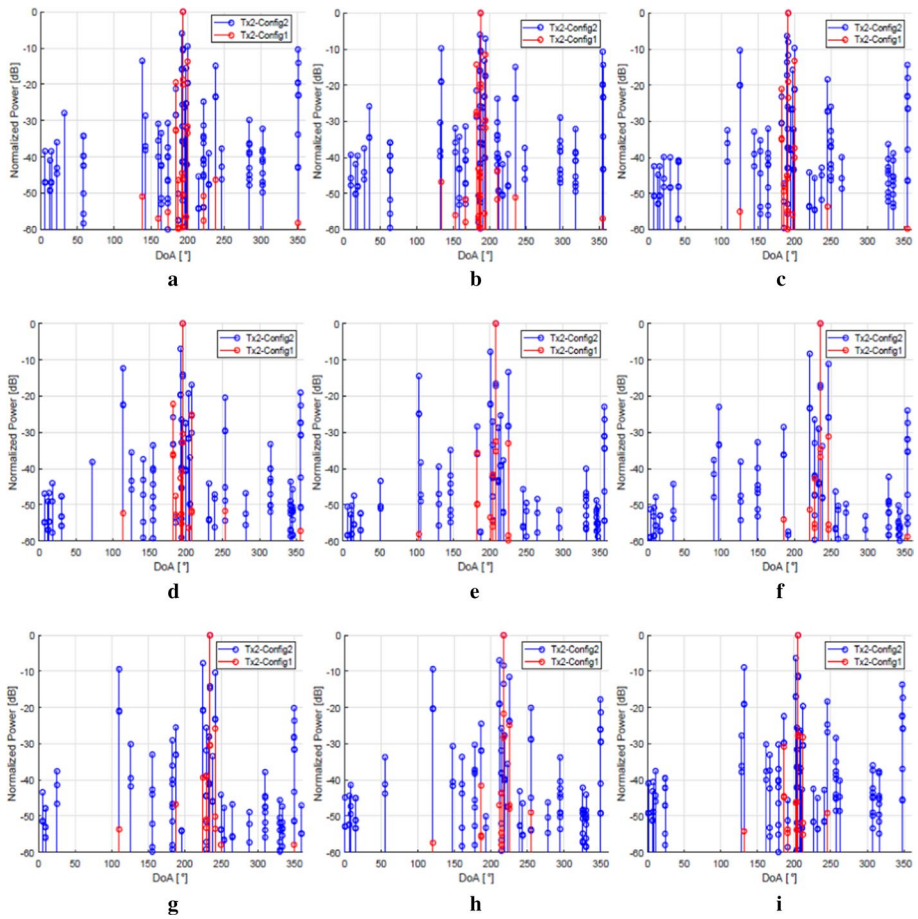

Fig. 17 Power angular profile with Tx2. **a** Pos 1, **b** Pos 2, **c** Pos 3, **d** Pos 4, **e** Pos 5, **f** Pos 6, **g** Pos 7, **h** Pos 8, and **i** Pos 9

Abbreviations

3D: Three dimensional; 5G: Fifth generation; DO: Direct orientation; DoA: Direction of arrival; eMBB: Enhanced mobile broad band; HPBW: Half power beamwidth; IT: Image theory; LoS: Line of sight; mmWave: Millimeter wave; PAP: Power angular profile; PDP: Power delay profile; PLO: Phase lock oscillator; RMS-AS: Root mean square angular spread; RMS-DS: Root mean square delay spread; RT: Ray tracing; Rx: Receiver; SBR: Shoot and bouncing; STD: Standard deviation; Tx: Transmitter; VNA: Vector network analyzer.

Acknowledgements

Not applicable.

Authors' contributions

MUS is the first and corresponding author of this article. The ray tracing tool used in the research work of this study is developed by MUS, and he contributed in the post processing and analysis of the simulation results, and took a lead role in writing of the paper. KR is the second author of the paper, and he contributed in drafting this work and was involved in the processing of the results. RJ is the third author of this work, he was involved in the conception and design of the work, and also contributed in the writing and proof reading of the paper. JH is the fourth author of this paper, he was involved in the drafting and writing of the paper and did proof reading of the manuscript. All authors collectively investigated the acquired results and were actively involved in discussions. All authors read and approved the final manuscript.

Authors' Information

Muhammad Usman Sheikh received his M.Sc. degree with Distinction and D.Sc. (Tech.) degree from Tampere University of Technology in 2009 and 2014, respectively. Currently, he is working as a post-doctoral researcher at Aalto University. His general interests include network planning and optimization, future mobile technologies, radio propagation, 3D ray tracing, advanced antennas and innovative cellular concepts.

Kalle Ruttik received the Diploma degree in engineering from Tallinn Technical University, in 1993, and the Lic.Tech. degree from the Helsinki University of Technology, in 1999. He received his D.Sc. (Tech.) degree in Telecommunications

Technology from Aalto University in 2011. He is currently a Teaching Researcher with the Department of Communications and Networking (ComNet), School of Electrical Engineering, Aalto University. His research interests include radio physical layer algorithms, software radio and cloud RAN.

Riku Jäntti received his D.Sc. (Tech.) degree (with distinction) in automation and systems technology in 2001. He is a full professor of communications engineering and the head of the Department of Communications and Networking at Aalto University. He is an associate editor of IEEE TVT. He was also IEEE VTS Distinguished Lecturer (Class 2016). His research interests include machine-type communications, cloud-based radio access networks, ambient backscatter communication and quantum communication.

Jyri Hämäläinen received his Ph.D. degree in Applied Mathematics in 1998 from University of Oulu and D.Sc. (Tech.) degree with honors in Signal Processing for Communications in 2007 from Helsinki University of Technology. He is a full professor and currently serving as a Dean of the School of Electrical Engineering at Aalto University. He received Good Teacher Award in 2009. His research interests include the design and analysis of wireless networks.

Funding
This work was partly supported by the Finnish public funding agency for research, Business Finland under the project "5G Finnish Open Research Collaboration Ecosystem (5G-FORCE)" which is part of 5G Test Network Finland.

Availability of data and materials
The datasets used and/or analyzed during the current study are available from the corresponding author on reasonable request.

Declarations

Competing interests
The authors declare that they have no competing interests

Received: 3 November 2020 Accepted: 24 March 2021
Published online: 07 April 2021

References

1. M. Xiao, S. Mumtaz, Y. Huang, L. Dai, Y. Li, M. Matthaiou, G.K. Karagiannidis, E. Björnson, K. Yang, I. Chih-Lin, A. Ghosh, Millimeter wave communications for future mobile networks. IEEE J. Sel. Areas Commun. **35**, 1909–1935 (2017)
2. S. Rangan, T.S. Rappaport, E. Erkip, Millimeter-wave cellular wireless networks: potentials and challenges. Proc. IEEE **102**(3), 366–385 (2014)
3. T.S. Rappaport, J.N. Murdock, F. Gutierrez, State of the art in 60-GHz integrated circuits and systems for wireless communications. Proc. IEEE **99**(8), 1390–1436 (2011)
4. T.S. Rappaport, Y. Xing, G.R. MacCartney, A.F. Molisch, E. Mellios, J. Zhang, Overview of millimeter wave communications for fifth-generation (5G) wireless networks with a focus on propagation models. IEEE Trans. Antennas Propag. **65**(12), 6213–6230 (2017)
5. S. Geng, J. Kivinen, X. Zhao, P. Vainikainen, Millimeter-wave propagation channel characterization for short-range wireless communications. IEEE Trans. Veh. Technol. **58**(1), 3–13 (2009)
6. P. Zhou, K. Cheng, X. Han, X. Fang, Y. Fang, R. He, Y. Long, Y. Liu, IEEE 802.11ay-based mmWave WLANs: design challenges and solutions. IEEE Commun. Surv. Tutor. **3**, 1654–1681 (2018)
7. V. Semkin, A. Karttunen, J. Jarvelainen, S. Andreev, Y. Koucheryavy, Static and dynamic millimeter-wave channel measurements at 60 GHz in a conference room, in *12th European Conference on Antennas and Propagation (EuCAP 2018)* (2018), pp. 1–5
8. S. Soni, A. Bhattacharya, An efficient two-dimensional ray-tracing algorithm for modeling of urban microcellular environments. Int. J. Electron. Commun. **66**(6), 439–447 (2012)
9. H.W. Son, N.H. Myung, A deterministic ray tube method for microcellular wave propagation prediction model. IEEE Trans. Antennas Propag. **47**(8), 1344–1350 (1999)
10. R.A. Kipp, M.C. Miller, Shooting-and-bouncing Ray method for 3D indoor wireless propagation in WLAN applications, in *IEEE Antennas and Propagation Society Symposium*, vol. 2 (2004), pp. 1639–1642
11. D. He, B. Ai, K. Guan, L. Wang, Z. Zhong, T. Kurner, The design and applications of high-performance ray-tracing simulation platform for 5G and beyond wireless communications: a tutorial. IEEE Commun. Surv. Tutor. **21**(1), 10–27 (2019)
12. M.E. Diago-Mosquera, A. Aragon-Zavala, G. Castanon, Bringing it indoors: a review of narrowband radio propagation modeling for enclosed spaces. IEEE Access **8**(1), 103875–103899 (2020)
13. A. Zhou, J. Huang, J. Sun, Q. Zhu, C. Wang, Y. Yang, 60 GHz channel measurements and Ray tracing modeling in an indoor environment, in *The 9th International Conference on Wireless Communications and Signal Processing (WCSP)* (2017), pp. 1–6
14. M. Peter, W. Keusgen, R. Felbecker, Measurement and Ray-tracing simulation of the 60 GHz indoor broadband channel: model accuracy and parameterization, in *The Second European Conference on Antennas and Propagation, EuCAP 2007* (2007), pp. 1–8

15. J. Pascual-Garcia, M. Martinez-Ingles, J.M. Garcia-Pardo, J. Rodriguez, L. J. Llácer, Using tuned diffuse scattering parameters in ray tracing channel modeling, in *The 9th European Conference on Antennas and Propagation (EuCAP)* (2015), pp. 1–4
16. M.U. Sheikh, J. Säe, J. Lempiäinen, Multipath propagation analysis of 5G systems at higher frequencies in Courtyard (small cell) environment, in *The IEEE 5G World Forum (5GWF)* (2018), pp. 239–243
17. M.U. Sheikh, J. Lempiäinen, Analysis of multipath propagation for 5G system at higher frequencies in microcellular environment, in *The 13th International Wireless Communications and Mobile Computing Conference (IWCMC)* (2017), pp. 1660–1664
18. B. Neekzad, K. Sayrafian-Pour, J. Perez, J.S. Baras, Comparison of ray tracing simulations and millimeter wave channel sounding measurements, in *The 18th International Symposium on Personal, Indoor and Mobile Radio Communications* (2007), pp. 1–5
19. M.J. Kazemi, A. Abdipur, A. Mohammadi, Indoor propagation MIMO channel modeling in 60 GHz using SBR based 3D ray tracing technique, in *The Second Conference on Millimeter-Wave and Terahertz Technologies (MMWaTT)* (2012), pp. 25–28
20. A.A. AlAbdullah, N. Ali, H. Obeidat, R.A. Abd-Alhmeed, S. Jones, Indoor millimetre-wave propagation channel simulations at 28, 39, 60 and 73 GHz for 5G wireless networks, in *The Internet Technologies and Applications (ITA)* (2017), pp. 235–239
21. M.U. Sheikh, K. Ruttik, R. Jäntti, J. Hämäläinen, Measurements and ray tracing simulations: impact of different antenna positions on meeting room coverage at 60 GHz, in *European Conference on Networks and Communications (EuCNC)* (2020), pp. 63–67
22. M. El Hajj, G. Zaharia, G. El Zein, H. Farhat, S. Sadek, Millimeter-wave propagation measurements at 60 GHz in indoor environments, in *International Symposium on Signals, Circuits and Systems (ISSCS)* (2019), pp. 1–4
23. A-INFO. Horn antenna. Accessed: 21-02-2021. [Online]. http://www.ainfoinc.com.cn/en/p_ant_h.asp
24. R. Zhang, X. Lu, J. Zhao, L. Cai, J. Wang, Measurement and modeling of angular spreads of three-dimensional urban street radio channels. IEEE Trans. Veh. Technol. **66**(5), 3555–3570 (2017)

Publisher's Note